

Humidity-Induced Phase Transitions in Ion-Containing Block Copolymer Membranes

Moon Jeong Park,^{†,§} Alisyn J. Nedoma,[†] Phillip L. Geissler,^{‡,||,¶} and Nitash P. Balsara^{*,†,§,#}

Department of Chemical Engineering and Department of Chemistry, University of California, Berkeley, California 94720, and Materials Sciences Division, Physical Biosciences Division, Chemical Sciences Division, and Environmental Energy Technologies Division, Lawrence Berkeley National Laboratory, University of California, Berkeley, California 94720

Andrew Jackson

NIST Center for Neutron Research, National Institute of Standards and Technology, Gaithersburg, Maryland 20899, and Department of Materials Science and Engineering, University of Maryland, College Park, Maryland 20742

David Cookson

Australian Synchrotron Research Program, Bldg 343, Advanced Photon Source, Argonne National Laboratory, 9700 South Cass Avenue, Argonne, Illinois 60439

Received October 18, 2007; Revised Manuscript Received January 3, 2008

ABSTRACT: The phase behavior of ion-containing block copolymer membranes in equilibrium with humidified air is studied as a function of the relative humidity (RH) of the surrounding air, ion content of the copolymer, and temperature. Increasing RH at constant temperature results in both disorder-to-order and order-to-order transitions. In-situ small-angle neutron scattering experiments on the open block copolymer system, when combined with water uptake measurement, indicate that the disorder-to-order transition is driven by an increase in the partial molar entropy of the water molecules in the ordered phase relative to that in the disordered phase. This is in contrast to most systems wherein increasing entropy results in stabilization of the disordered phase.

Introduction

There is a growing need to characterize phase transitions of open systems wherein the chemical potential of the species being exchanged between the system and the surrounding bath becomes an important variable. An example of a physical system where such information is important is a fuel cell. Fuel cells that use hydrogen and air as inputs and produce electric power and water as outputs are of particular significance due to their potential to serve as clean energy sources. Polymer electrolyte membranes (PEM) such as Nafion are used to conduct protons from the anode to the cathode.^{1–4} PEMs, comprising amphiphilic chain molecules with hydrophobic and hydrophilic segments, are open systems that exchange water with the surrounding air and their proton conductivity is closely coupled to the presence of contiguous hydrated channels within the membrane. While order–order and order–disorder transitions (OOT and ODT, respectively) in systems containing amphiphilic molecules such as phospholipids, surfactants, and block copolymers have been the subject of extensive research,^{5–10} they are typically studied in closed systems at a fixed composition. The purpose of this paper is to present results of a fundamental study of temperature- and humidity-induced OOTs and ODTs in an open block copolymer-based PEM system at equilibrium with humid air.

To our knowledge, all previous studies of ion-containing block copolymers in the presence of humid air are restricted to microphase-separated systems.^{11–13} Accessing the disordered state is of fundamental importance as the entropic and energetic driving forces for order formation are balanced at the order–disorder transition. Flory–Huggins interaction parameters, χ , are routinely used to describe polymer/polymer and polymer/solvent interactions.^{14–17} In most cases, χ between polymer chains decreases with increasing temperature, and when it decreases below a certain critical value, a transition from order-to-disorder is observed. In pioneering studies, Lodge et al. showed that the phase behavior of mixtures of block copolymers and selective organic solvents can be understood in terms of effective polymer–polymer χ parameters.¹⁸ The extent to which such a framework applies to systems where the selective solvent is water remains to be established.

Here, we show that increasing the relative humidity (RH) of the air surrounding a block copolymer membrane results in a disorder-to-order transition at fixed temperature. In particular, at fixed RH above 54%, increasing temperature leads to a disorder-to-order transition. This is in contrast to data obtained from the dry block copolymer, where increasing temperature leads to an order-to-disorder transition. We show that this qualitative difference arises because the partial molar entropy of water dominates the thermodynamic properties of the moist membranes.

Experimental Section²⁶

Polymer Synthesis and Characterization. A polystyrene–polyisoprene block copolymer with polydispersity index of 1.03

* Corresponding author.

[†] Department of Chemical Engineering, UC Berkeley.

[‡] Department of Chemistry, UC Berkeley.

[§] Materials Sciences Division, Lawrence Berkeley National Laboratory.

^{||} Physical Biosciences Division, Lawrence Berkeley National Laboratory.

[¶] Chemical Sciences Division, Lawrence Berkeley National Laboratory.

[#] Environmental Energy Technologies Division, Lawrence Berkeley National Laboratory.

was synthesized and characterized using methods described in ref 19. Selective hydrogenation of the polyisoprene block was conducted in the presence of a homogeneous Ni–Al catalyst with cyclohexane as the solvent, using a 2 L Parr batch reactor at 83 °C and 420 psi, following procedures given in ref 9. The hydrogenation reaction was repeated about four times until no detectable diene group was observed in the ^1H nuclear magnetic resonance (NMR in d_6 -acetone) spectrum of the polymer. All of the NMR experiments were conducted on a 500 MHz Bruker AV500 spectrometer. The NMR spectra also confirmed that the styrene units were not saturated, and gel permeation chromatography confirmed that there was no chain degradation. The hydrogenated block copolymers are referred to as poly(styrene–methylbutylene) (PS–PMB) copolymers. The number-averaged molecular weights of the blocks of the PS–PMB copolymer are $M_{n,PS} = 1.4$ kg/mol and $M_{n,PMB} = 1.4$ kg/mol. We use the term P1 to refer to these polymers where 1 is the nominal molecular weight of each of the blocks in kg/mol. The PS block of the PS–PMB copolymer was sulfonated using procedures described in ref 16. Samples with different degrees of sulfonation were prepared by controlling reaction time. The polymer in the reaction mixture was purified by dialysis against pure water using a cellulose dialysis membrane with a 3.5 kg/mol molecular weight cutoff (VWR) for 10 days. Some polymer is lost in this step as the polymer molecular weight is below the cutoff of the dialysis membrane. Controlling the time required for this step is crucial as waiting too long results in loss of the polymer sample while waiting for only a short period of time results in acid contamination of the polymer. NMR measurements were used to determine the acid concentration in the polymer as it was dialyzed. The polymer was then recovered by vacuum drying at 60 °C for 7 days. The sulfonated block copolymers are referred to as polystyrenesulfonate–polymethylbutylene (PSS–PMB) copolymers.

It is customary in the literature to use ion-exchange capacity (IEC) to quantify sulfonation levels. The IEC value quantifies the moles of sulfonic acid (SA) groups per gram of polymer (mmol/g) and is defined as

$$\text{IEC} = \frac{\text{mol of SA}}{\text{mol of SA} \times 185.23 + \text{mol of S} \times 104.15 + \text{mol of MB} \times 70.12} \quad (1)$$

Samples are labeled according to the IEC; for example, P1(1.513) has IEC = 1.513 mmol/g with 30 mol % sulfonation level while P1(0) refers to the unsulfonated PS–PMB copolymers.

Small-Angle X-ray Scattering (SAXS). 1 mm thick PSS–PMB samples were prepared by solvent-casting using THF as a solvent under nitrogen blanket for 2 days followed by vacuum drying at 50 °C for 10 days. Synchrotron SAXS measurements were performed using the 15-ID-D beamline at the Advanced Photon Source (APS). Sample temperature was controlled within ± 0.2 °C using a sample stage provided by the APS. Samples were equilibrated for at least 15 min before measurement. The resulting two-dimensional scattering data were averaged azimuthally to obtain intensity vs magnitude of the scattering wave vector q ($q = 4\pi \sin(\theta/2)/\lambda$, where θ is the scattering angle). The scattering data were corrected for the CCD dark current and the scattering from air and Kapton windows.

Transmission Electron Microscopy (TEM). The PSS–PMB samples prepared by the same method used to prepare the SAXS samples were cryo-microtomed at -100 °C to obtain thin sections with thicknesses in the 50 – 80 nm range using an RMC Boeckeler PT XL ultramicrotome. The electron contrast in the dry polymer samples was enhanced by exposure to ruthenium tetroxide (RuO_4) vapor for 50 min. Imaging of stained samples was performed with a Zeiss LIBRA 200FE microscope operating at 200 kV equipped with a cold stage (-160 °C) and an Omega energy filter. To prevent beam damage, the polymer sections evacuated at 10^{-5} Pa were placed on the cold stage before they were exposed to the electron beam. Images were recorded on a Gatan 2048 \times 2048 pixel CCD camera (Gatan Inc., Pleasanton, CA). All data sets were acquired using Digital Micrograph (Gatan, Inc.) software. The TEM images

thus enable quantification of the room-temperature morphology of our PSS–PMB copolymers.

In-Situ Small-Angle Neutron Scattering (In-Situ SANS). The SANS samples were prepared by solvent-casting the polymer from THF solutions on 1 mm quartz windows. The sample thickness ranged from 50 to 130 μm and a circular area with a diameter of 1.59 cm was exposed to the neutron beam. The samples were studied using the 30 m NG7 beamline at the National Institute of Standards and Technology (NIST) equipped with a sample holder wherein the humidity of the surrounding air and sample temperature were controlled. Water from a well located within the sample chamber is used to humidify the air around the sample. In our experiments, the well was filled with pure D_2O . The wavelength of the incident neutron beam (λ) was 0.6 nm ($\Delta\lambda/\lambda = 0.10$), and sample-to-detector distances of 1.0, 3.0, and 12.0 m were used. This enabled access to scattering at q values in the range 0.03–5.9 nm^{-1} . The uncertainty of the sample humidity and temperature for the NIST humidity sample chamber are $\pm 1\%$ RH and ± 1 °C, respectively. Samples were equilibrated for at least 5 min before measurement. Separate transient measurements were conducted as a function of sample thickness to ensure that this equilibration time was adequate for the temperature and humidity steps used in our study.

Water Uptake Measurements. Polymer films with thickness ranging from 50 to 70 μm were prepared by solvent casting from 10 wt % THF solutions. The films were dried at room temperature for 3 days under a N_2 blanket and under vacuum at 60 °C for 5 days. Prior to water uptake experiments, the films were exposed to vacuum for 24 h and then hooked on the end of the quartz spring balance (RUSKA, spring constant $k = 4.9$ mN/m), located in an ESPEC SH-241 humidity chamber equipped with specially designed glassware to prevent breakage of the quartz spring due to air flow in the humidity chamber. The spring is nonrotating and has a reference pointer, which is used to measure the increment of total length of the spring upon hydration. Samples were studied as a function of temperature ranging from 25 to 90 °C and RHs from 50 to 98%. The water uptake is calculated using the dry film as the basis:

$$\text{water uptake} = \frac{\text{weight of wet film} - \text{weight of dry film}}{\text{weight of dry film}} \times 100\% \quad (2)$$

The reported water uptake values are based on measurements from five independent samples. The standard deviation of the measurements was less than 5% of the averaged values. We also carried out water uptake measurements using a Mettler balance with 0.01 mg accuracy. Differences between the two measurements were within $\pm 2.5\%$.

Differential Scanning Calorimetry (DSC). DSC experiments were performed with a TA Instruments DSC model 2920 with a heating rate of 1 °C/min. The instrument was calibrated using indium, zinc, and tin. For the measurement, ~ 10 mg of dry polymer was encapsulated in an aluminum pan using a sample press and run against an empty aluminum reference pan.

Results and Discussion

The phase behavior of the P1 series in contact with ambient air, air with an approximate relative humidity, RH = 32%, was characterized by synchrotron SAXS and cross-sectional TEM. The water concentration in the polymer under these conditions is expected to be less than 3 wt % on the basis of the extrapolation of water uptake results. In-situ SANS measurements (described below) show that humidity of the surrounding air affects the phase behavior of PSS–PMB only when RH > 54%. For simplicity, we refer to the characteristics of PSS–PMB in contact with ambient air as those of dry PSS–PMB copolymers. Figure 1a shows SAXS profiles for the P1 series as a function of IEC at 22 °C. P1(0) is a completely disordered low-viscosity liquid. Consequently, it is not surprising that the SAXS profile of P1(0) is featureless. Increasing the IEC value

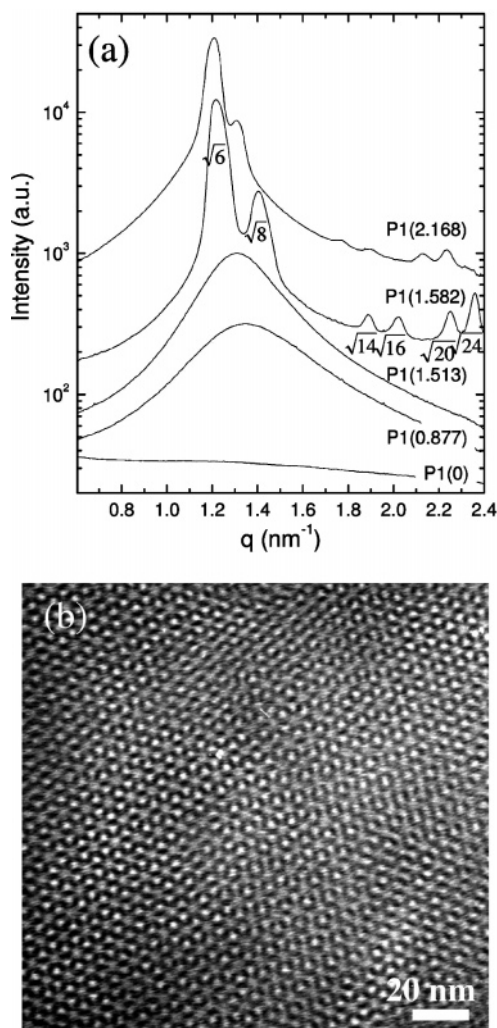


Figure 1. (a) SAXS profiles of P1 series as a function of IEC at 22 °C and (b) cross-sectional TEM image of P1(1.582). Scattering profiles are offset vertically by factors of 2, 2², 2⁴, and 2⁶ for clarity. PSS domains were darkened by RuO₄ staining.

from 0 to 1.513 results in the appearance of a broad SAXS peak, characteristic of disordered block copolymers. A slight increase in IEC from 1.513 to 1.582 mmol/g induces a morphological transformation from a disordered state to an ordered gyroid structure. This increase in IEC also results in the solidification of polymer P1. The Bragg peaks at $\sqrt{6}q^*$, $\sqrt{8}q^*$, $\sqrt{14}q^*$, $\sqrt{16}q^*$, $\sqrt{20}q^*$, and $\sqrt{24}q^*$, where $q^* = 2\pi/d_{211}$ (d = domain spacing) with $d_{211} = 5.15$ nm, seen in Figure 1a are consistent with the $Ia\bar{3}d$ space group. The Miller indices corresponding to the observed Bragg peaks are (211), (220), (321), (400), (420), and (422).²⁰ The gyroid structure is observed over a wide range of IEC values, up to 2.168 mmol/g.

This gyroid morphology was also clearly observed by TEM. The cryo-microtomed sections were vacuum-dried before the experiments, and the electron contrast in dry samples was enhanced by exposure to ruthenium tetroxide (RuO₄) vapor by staining styrene units. Figure 1b shows TEM results from P1(1.582) where the wagon-wheel structure, typically obtained from gyroid samples, is seen. The dimensions of the unit cell as measured by SAXS and TEM are in reasonable agreement. For example, the spacing of the {211} planes (5.2 nm) obtained by SAXS corresponds to half the “spoke” length observed in TEM (4.8 nm).

To our knowledge, the smallest block copolymer to exhibit an ordered phase in previous literature is a polyethylene-*block*-

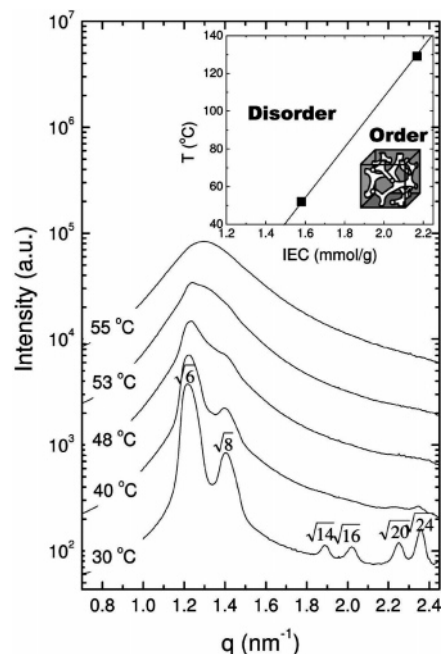


Figure 2. SAXS profiles of the P1(1.582) as a function of temperature indicating ODT at 54 °C. Scattering profiles are offset vertically by factors of 3.3, 3.3², 3.3³, and 3.3⁴ for clarity. The inset shows the phase diagram of P1 series as a function of IEC value.

poly(ethylene oxide) (PE–PEO) copolymer with 0.83 and 0.90 kg/mol PE and PEO blocks, respectively, studied in ref 21. This PE–PEO copolymer was disordered above the melting point of the PE and PEO crystals; i.e., microphase separation was driven entirely by the crystallinity of PE and PEO chains and not thermodynamic repulsion between chains. Consequently, the domain spacing of lamellar structure for the PE–PEO copolymer, which ranged from 7.5 to 11.0 nm, is considerably larger than that expected from typical data obtained from amorphous block copolymers. In comparison, the domain spacing of the gyroid phase of P1(1.582) is 5.2 nm. To our knowledge, the ordered phase in P1(1.582) is the smallest ordered structure obtained by self-assembly in block copolymers.

The SAXS intensity at all accessible q values decreases monotonically with increasing temperature, irrespective of the sulfonation level of the copolymer. This is illustrated in Figure 2, where we show SAXS profiles of P1(1.582) at selected temperatures. The higher order peaks of P1(1.582), indicative of the gyroid phase, disappear at a temperature between 53 and 55 °C. The ODT temperature, T_{ODT} , of P1(1.582), is thus 54 ± 1 °C. The T_{ODT} of P1(2.168) is seen at 119 ± 1 °C. The methodology outlined above was used to map out the phase diagram of the dry P1 series as a function of temperature and IEC, and the resulting phase diagram is shown in the inset of Figure 2. Throughout this paper we use parsimonious interpolations and extrapolations to connect individual phase boundary data points, as is the case in the inset of Figure 2.

In-situ small-angle neutron scattering (in-situ SANS) data were obtained from P1 samples placed in a humidity- and temperature-controlled sample environment ($\pm 1\%$ RH and ± 1 °C) at the 30 m NG7 beamline at the NIST. The lowest RH limit and the highest temperature limit of the NIST environmental chamber are RH = 25% and $T = 80$ °C, respectively. The protocols needed to establish equilibrium after changing the temperature and humidity of the surrounding air were determined in independent experiments.²² When a 123 μm thick P1(1.513) film was exposed to a D₂O/air environment at fixed temperature of 25 °C, as shown in Figure 3a, the broad primary

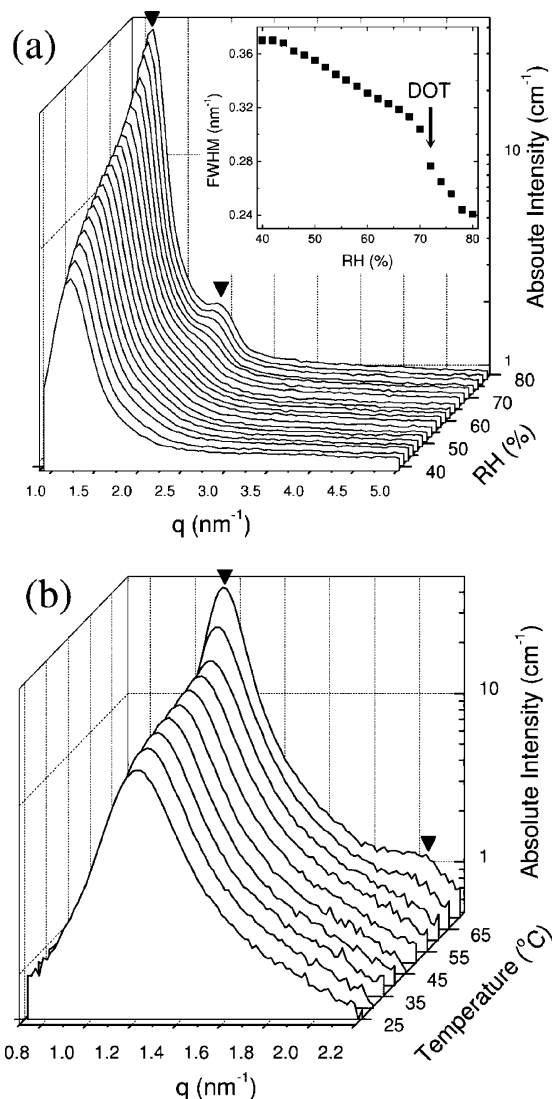


Figure 3. (a) In-situ SANS profiles of P1(1.513) as a function of RH at 25 °C showing humidity-induced disorder-to-order transition. Inset shows a discontinuous change in fwhm of the primary scattering peak at RH = 70%. (b) In-situ SANS profiles of P1(1.513) as a function of temperature at RH = 60%, indicating a temperature-induced disorder-to-order transition.

peak indicative of a disordered phase was seen at low humidity. The scattering intensity increases significantly with increasing RH due to the increase in D₂O concentration within the polymer and the concomitant increase in the scattering contrast between the hydrophobic and hydrophilic microphases. When the RH is increased from 70 to 72%, we see the $1q^*$ and $2q^*$ Bragg reflections with $q^* = 1.15 \text{ nm}^{-1}$, indicating the presence of a lamellar phase with domain spacing $d_{100} = 5.46 \text{ nm}$. The humidity at which the disorder-to-order transition (DOT) takes place was determined by noting the humidity jump that causes a discontinuous change in the full width at half-maximum (fwhm) of the primary peak, as shown in the inset of Figure 3a.

Typical temperature-dependent in-situ SANS profiles at a fixed humidity are shown in Figure 3b, where data obtained from P1(1.513) at RH = 60% D₂O vapor are shown. The peak intensity increases monotonically with increasing temperature up to a temperature of 60 °C. Heating the sample to 65 °C results in an abrupt decrease in fwhm of the peak and the appearance of the $2q^*$ peak corresponding to the lamellar phase. Note that in the dry state (ambient humidity) increasing temperature leads

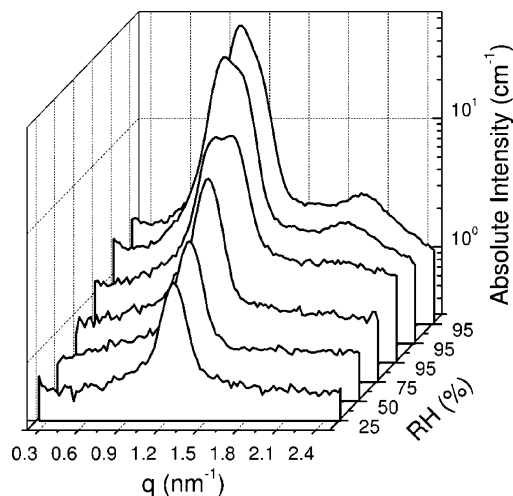


Figure 4. In-situ SANS profiles of P1(1.582) as a function of RH at 25 °C showing a humidity-induced gyroid-to-lamellar transition. The three profiles at 95 °C were obtained as a function of time (t) after RH was switched from 75 to 95%; $t = 30, 60,$ and 120 min .

to a decrease in SAXS intensity, regardless of IEC value, and stabilizes the disordered state in samples where the DOT is accessible. In contrast, increasing temperature results in an increase in the SANS intensity and stabilizes the ordered phase in P1(1.513) at RH = 60%. Similar effects were observed at other RH values: $T_{\text{DOT}} = 75 \text{ °C}$ at RH = 54%, $T_{\text{DOT}} = 50 \text{ °C}$ at RH = 65%, and $T_{\text{DOT}} = 35 \text{ °C}$ at RH = 70%. It is evident that the presence of moist air has a qualitative effect on the nature of phase transitions in block copolymers.

Exposing a dry 97 μm thick P1(1.582) sample with a gyroid morphology to increasingly moist air resulted in a humidity induced OOT to a lamellar morphology at RH = 95%, as shown in Figure 4. The lack of higher order peaks in the SANS profile at RH = 25% is due to well-known differences in the resolution of SAXS and SANS instruments.²³ The scattering intensity increases with increasing RH up to RH = 75%. When RH was further increased to RH = 95%, we observed the nucleation and growth of a lamellar phase with $d = 5.98 \text{ nm}$. The primary scattering peak of the lamellar phase is distinct from that of the gyroid phase, and this facilitates tracking the gyroid-to-lamellae phase transition. It takes about 2 h to complete the transition. At intermediate times peaks corresponding to both gyroid and lamellar phases were evident (Figure 4).

The methodology described above was used to map out the phase behavior of a variety of P1 samples, and the results are summarized in Figure 5a–c using T vs RH plots at fixed IEC values. The letters D, L, and G indicate disorder, lamellae, and gyroid phases, respectively. The DOTs and OOTs are indicated by squares, and the solid lines show the phase boundaries. At a low IEC value of 0.877 we see disorder over most of the T –RH window with a lamellar phase in the high T , high RH corner. At an intermediate IEC value of 1.513 the T –RH window is more-or-less equally divided between disorder at low temperature and a lamellar phase at high temperature. Qualitatively different behavior is seen at a high IEC value of 1.582, where a gyroid phase is seen at low temperatures and a lamellar phase is seen at high temperatures.

The phase behavior of P1 as a function of temperature, IEC, and humidity of the surrounding air, was obtained by the combination of experiments described above, and the results are plotted inside a cube in Figure 5d. The left and back surface of the cube at RH = 25% represents the phase behavior in the dry state, plotted as temperature vs the IEC value, and is

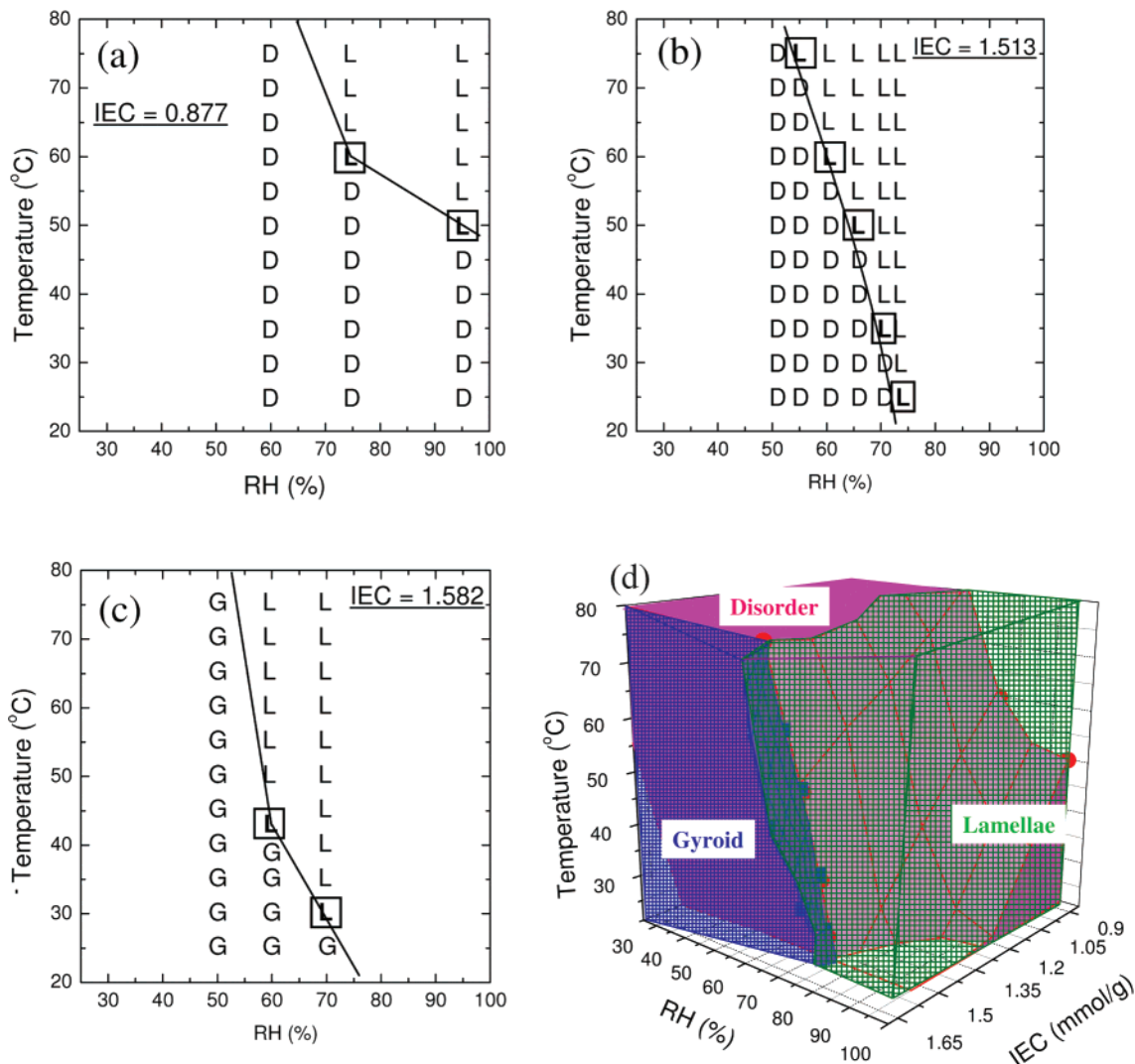


Figure 5. (a–c) Phase diagrams of P1 samples as a function of T and RH at given IEC values. D, L, and G indicate disorder, lamellae, and gyroid phases, respectively. The DOTs and OOTs are marked with squares and the solid lines. (d) 3-dimensional phase cube of P1 block copolymer as a function of temperature, T , relative humidity of the surrounding air, RH, and ion content, IEC.

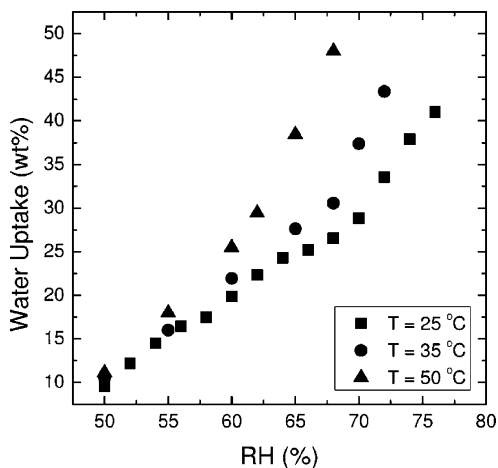


Figure 6. Water uptake results from P1(1.513) as a function of humidity at $T = 25, 35,$ and $50\text{ }^\circ\text{C}$.

identical in content to the inset of Figure 2. The third axis of the cube represents changes in RH. The disordered phases occupy the low IEC and low RH section of the cube. The gyroid phase is mainly seen at low RH while the lamellar phases are seen at high RH. In Figure 5b, the surfaces between disorder/

lamellae and gyroid/lamellae within the cube were obtained using a Renka-Cline gridding algorithm, which is part of the OriginPro 7.5 software package.

The results of water uptake measurements on P1(1.513) as a function of T and RH are shown in Figure 6. These measurements combined with the in-situ SANS data enable determination of structure as a function of water concentration inside the polymer. The results of this analysis are shown in Figure 7a, where T_{DOT} of P1(1.513) as a function of water concentration within the polymer. It is evident that T_{DOT} is a linear function of water concentration in the membrane, expressed as n_w/n_p , where n_w and n_p represent moles of water and block copolymer, respectively. The slope of the line is -1.15 K . We note in passing that the Gibbs phase rule requires coexistence regions at the phase boundaries. The width of these regions in our system are smaller than the steps used to study phase behavior and were thus within experimental resolution.

Equality of the chemical potential of water, μ_w , in the ordered and disordered phases along the coexistence line (e.g., Figure 7a), indicates that

$$\left(\frac{\partial\mu_w^{(O)}}{\partial T}\right)_{n_w} dT + \left(\frac{\partial\mu_w^{(O)}}{\partial n_w}\right)_T dn_w = \left(\frac{\partial\mu_w^{(D)}}{\partial T}\right)_{n_w} dT + \left(\frac{\partial\mu_w^{(D)}}{\partial n_w}\right)_T dn_w \quad (3)$$

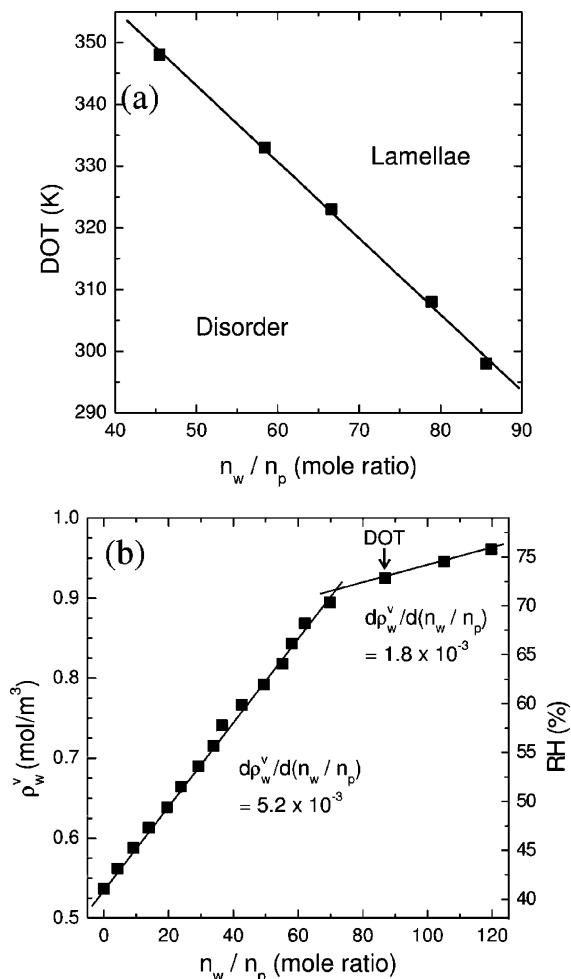


Figure 7. (a) Phase behavior of P1(1.513) as a function of molar ratio of water to polymer in the membrane (n_w/n_p). The n_w/n_p values were obtained from water uptake measurements shown in Figure 6. (b) Molar concentration of water in the surrounding air (ρ_w^v) at different RH values vs n_w/n_p at 25 °C. The DOT determined by in-situ SANS is indicated by an arrow.

where superscripts (O) and (D) represent ordered and disordered phases. Pressure and n_p , the other variables that determine μ_w , are assumed to be constant, as is the case in the experiments. Rearranging eq 3 and using Maxwell's equations gives

$$\frac{dT}{d(n_w/n_p)} = \frac{\Delta \left(\frac{\partial \mu_w}{\partial (n_w/n_p)} \right)_T}{\Delta s_w} \quad (4)$$

where s_w is the partial molar entropy of water, and Δ refers to the difference between the quantity of interest in the ordered and disordered states, respectively.

Assuming that the surrounding air obeys ideal gas behavior, the chemical equilibrium of water in the membrane and the water vapor in the surrounding air leads to the following expression:

$$\mu_w = \mu_w^v = \mu_w^0 + RT \ln \left(\frac{\rho_w^v}{\rho_w^0} \right) \quad (5)$$

where superscript v stands for the vapor phase, ρ_w^v is the concentration of water vapor in the air (moles per unit volume), and the superscript 0 refers to the standard state. Taking the derivative of μ_w in eq 5 gives

$$\left(\frac{\partial \mu_w}{\partial n_w/n_p} \right)_T = \frac{RT}{\rho_w^v} \left(\frac{\partial \rho_w^v}{\partial n_w/n_p} \right)_T \quad (6)$$

The water-uptake measurements can be recast to give the dependence of ρ_w^v vs n_w/n_p . ρ_w^v vs n_w/n_p data of P1(1.513) at 25 °C are shown in Figure 7b. Note that eqs 4 and 6 indicate that there is a change in the slope in the ρ_w^v vs n_w/n_p data at the humidity-induced DOT at constant temperature. This is in reasonable agreement with the data in Figure 7b. The SANS data indicate that the DOT occurs at $n_w/n_p = 87 \pm 1$, while the change in slope of the ρ_w^v vs n_w/n_p occurs at $n_w/n_p = 77 \pm 8$. We offer no substantive explanation for the slight difference in the DOTs seen in the SANS and water uptake measurements, other than to note the vast difference in instrumentation, humidity control, and the use of D_2O in SANS and H_2O in the water uptake experiments. Least-squares linear fits through the ρ_w^v vs n_w/n_p data obtained in the ordered and disordered states give $\Delta[\partial \mu_w / \partial (n_w/n_p)]_{DOT} = -8.10$ J/mol. Using eq 6 along with the measured slope of the $dT/d(n_w/n_p)$ data enables a measure of Δs_w , which for P1(1.513) is 7.04 J/(mol K). Using the same analysis for the other accessible DOTs led to estimates of Δs_w of 4.62 and 5.86 J/(mol K) at $T = 35$ °C and $T = 50$ °C, respectively. The average value of Δs_w is 5.84 J/(mol K).

Note that the sign of Δs_w is nontrivial. It indicates that the s_w in the ordered state is higher than that in the disordered state.

We estimated Δs_p , the difference between the partial molar entropy of the polymer chains in the ordered and disordered states, by conducting DSC on dry P1(1.582) (in ambient air). We report data obtained during the second heating run at a rate of 1 °C/min in Figure 8. A clear endothermic peak is observed in the vicinity of T_{ODT} (60 °C), and the associated latent heat is 0.21 J/g. It is clear that the enthalpy difference between ordered and disordered states, ΔH , is negative, as is usually the case in block copolymers. Since $\Delta H = T\Delta S$ at the ODT, Δs_p of P1(1.582) is estimated to be -2.0 J/(mol K). The partial molar entropy change of polymer molecules has the usual sign. To obtain an estimate of the factors that govern the thermodynamic properties of PSS–PMB membranes in humid air, we assume that Δs_p is not affected by the presence of water or small changes in IEC. This enables determination of Δs_{total} , the total molar entropy of ordering of P1(1.513), as $\Delta s_{total} = (n_w \Delta s_w + n_p \Delta s_p) / (n_w + n_p) = 5.62$ J/(mol K), which is only slightly smaller than the average Δs_w value. It is clear that the total entropy of the system is dominated by that of the water molecules. DSC experiments on PSS–PMB systems under controlled humidity would provide more accurate estimates of Δs_p , but we did not have access to such instrumentation. While we have determined Δs_w for DOTs, it should be clear that the same methodology is, in principle, applicable to all of the phase boundaries plotted in Figure 5d.

It has been shown that the entropy of water molecules in hydrophobic environments depends crucially on the size of the hydrophobic moieties and entropic effects dominate when the size is less than 0.4 nm.²⁴ The smallest length scales of the hydrophilic domains in our samples are considerably larger than this limit. It is conceivable, however, that the hydrophilic domains are not homogeneous and that water is sequestered in small pools around the SO_3^- ionic groups. As a result, theories of the hydrophobic effect developed for bulk liquid may not directly apply. Heterogeneous distributions of ionic species in partially sulfonated homopolymers are well-established.²⁵ Experiments to see whether similar effects are present in our PSS–PMB copolymers are currently underway.

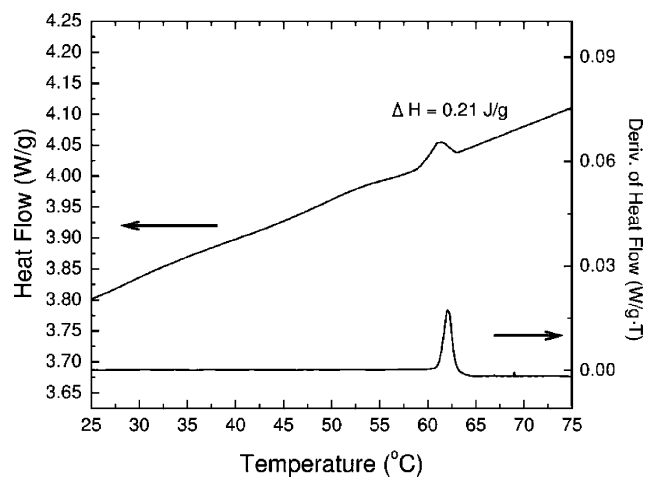


Figure 8. DSC trace obtained from PI(1.582) at a rate of 1 °C/min. The temperature dependencies of heat flow and the derivative of heat flow vs temperature are shown.

Conclusion

We have studied humidity-induced phase transitions in sulfonated block copolymers as a function of temperature, IEC, and humidity of the surrounding air. The phase behavior is mapped onto a 3-dimensional phase cube. The disordered phase occupies the low IEC and low RH section of the cube, and the gyroid phase is seen at the high IEC and low RH while the lamellar phases are seen at high RH. The change in the partial molar entropy of water in the moist polymer membranes upon ordering was quantified using general thermodynamic arguments that do not rely on specific microscopic models for describing the polymer mixture such as the Flory–Huggins theory or the random phase approximation. This was entirely due to the fact that our block copolymer was in equilibrium with a thermodynamically simple system—moist air which can be approximated as an ideal gas. It is, perhaps, worth noting, that the water content of the membrane exhibits a continuous change across the disorder–order transition, and thus Δs_w predicted on the basis of the Flory–Huggins theory would be identically zero. It is evident that conventional models based on the effective χ parameters¹⁸ are not appropriate for describing the thermodynamic properties of PSS–PMB systems at equilibrium with humid air. A complete understanding of the phase behavior of humidified block copolymers will require quantification of enthalpic driving forces that are not addressed here. Our work does, however, suggest the need for the development of radically new microscopic models that predict the thermodynamics of humidified block copolymers near order–disorder transitions.

Acknowledgment. Major funding for this work was provided through the Electron Microscopy of Soft Matter Program at Lawrence Berkeley National Laboratory (LBNL) supported by the Director, Office of Science, Office of Basic Energy Sciences, Materials Sciences and Engineering Division, of the

U.S. Department of Energy under Contract DE-AC02-05CH11231. TEM was performed at the National Center for Electron Microscopy at LBNL. SAXS measurements were conducted at the Advanced Photon Source (APS) supported by the U.S. Department of Energy, Office of Science, Office of Basic Energy Sciences, under Contract DE-AC02-06CH11357, on the ChemMatCARS Sector 15 instrument which is principally supported by the National Science Foundation/Department of Energy under Grant CHE-0535644. The SANS facilities at NIST are supported in part by the National Science Foundation under Agreement DMR-0504122.²⁶

References and Notes

- Hickner, M. A.; Ghassemi, H.; Kim, Y. S.; Einsla, B. R.; McGrath, J. E. *Chem. Rev.* **2004**, *104*, 4587.
- Mauritz, K. A.; Moore, R. B. *Chem. Rev.* **2004**, *104*, 4535.
- Kreuer, K. D. In *Handbook of Fuel Cell—Fundamentals, Technology and Applications*; Vielstich, W., Lamm, A., Gasteiger, H. A., Eds.; John Wiley & Sons Ltd.: Chichester, UK, 2003; Vol. 3, Part 3.
- Maréchal, M.; Souquet, J.-L.; Guindet, J.; Sanchez, J.-Y. *Electrochem. Commun.* **2007**, *9*, 1023.
- Leibler, L. *Macromolecules* **1980**, *13*, 1602.
- Fredrickson, G. H.; Helfand, E. *J. Chem. Phys.* **1987**, *87*, 697.
- Mayes, A. M.; Barker, J. G.; Russell, T. P. *J. Chem. Phys.* **1994**, *101*, 5213.
- Lodge, T. P.; Xu, X.; Ryu, C. Y.; Hamley, I. W.; Fairclough, J. P. A.; Ryan, A. J.; Pedersen, J. S. *Macromolecules* **1996**, *29*, 5955.
- Adams, J. L.; Quiram, D. J.; Graessley, W. W.; Register, R. A.; Marchand, G. R. *Macromolecules* **1998**, *31*, 201.
- Schwab, M.; Stühn, B. *Phys. Rev. Lett.* **1996**, *76*, 924.
- Won, J.; Park, H. H.; Kim, Y. J.; Choi, S. W.; Ha, H. Y.; Oh, I.-H.; Kim, H. S.; Kang, Y. S.; Jin, K. J. *Macromolecules* **2003**, *36*, 3228.
- Shi, Z.; Holdcroft, S. *Macromolecules* **2005**, *38*, 4193.
- Elabd, Y. A.; Napadensky, E.; Walker, C. W.; Winey, K. I. *Macromolecules* **2006**, *39*, 399.
- Huggins, M. L. *J. Chem. Phys.* **1941**, *9*, 440.
- Flory, P. In *Principles of Polymer Chemistry*; Cornell University Press: Ithaca, NY, 1953; Chapter XIII.
- Beck Tan, N. C.; Liu, X.; Briber, R. M.; Peiffer, D. G. *Polymer* **1995**, *36*, 1969.
- Zhou, N. C.; Xu, C.; Burghardt, W. R.; Composto, R. J.; Winey, K. I. *Macromolecules* **2006**, *39*, 2373.
- Hanley, K. J.; Lodge, T. P.; Huang, C.-I. *Macromolecules* **2000**, *33*, 5918.
- Balsara, N. P.; Lin, C. C.; Dai, H. J.; Krishnamoorti, R. *Macromolecules* **1994**, *27*, 1216.
- Benedicto, A. D.; O'Brien, D. F. *Macromolecules* **1997**, *30*, 3395.
- Sun, L.; Liu, Y.; Zhu, L.; Hsiao, B. S.; Avila-Orta, C. A. *Polymer* **2004**, *45*, 8181.
- Park, M. J.; Downing, K. H.; Jackson, A.; Gomez, E. D.; Minor, A. M.; Cookson, D.; Weber, A. Z.; Balsara, N. P. *Nano Lett.* **2007**, *7*, 3547.
- Jhao, J.; Majumdar, B.; Schulz, M. F.; Bates, F. S.; Almdal, K.; Mortensen, K.; Hajduk, D. A.; Gruner, S. M. *Macromolecules* **1996**, *29*, 1204.
- Chandler, D. *Nature (London)* **2005**, *437*, 640.
- O'Connell, E. M.; Root, T. W.; Cooper, S. L. *Macromolecules* **1995**, *28*, 4000.
- Certain commercial equipment, instruments, or materials (or suppliers, or software) are identified in this paper to foster understanding. Such identification does not imply recommendation or endorsement by the National Institute of Standards and Technology, nor does it imply that the materials or equipment identified are necessarily the best available for the purpose.

MA702320T